

Journal of Environmental & Earth Sciences

https://journals.bilpubgroup.com/index.php/jees

ARTICLE

Single Borehole Detection of Geological Anomalies in Coal Mine Using Impulse Radar

Zhenrong Wang 1,2 10 , Yuan Yang 1,2 10 , Fengjuan Tao 3* 10

ABSTRACT

Geological anomalies, including faults, fractured zones, and collapse pillars, pose serious threats to mining safety by increasing the risk of water inrush and roof collapse. To enable accurate ahead-of-face detection, this paper presents the development and practical application of a single-borehole impulse radar (BHR) system specifically designed for underground coal mine environments. The system incorporates a compact, explosion-proof probe constructed from fiberglass, with a diameter of 40 mm, making it suitable for deployment in confined boreholes. By leveraging wideband impulse signals, the BHR achieves high-resolution subsurface imaging while maintaining low power consumption and rapid data acquisition rates. The system's detection performance was first verified through controlled ground experiments in a railway tunnel, where it accurately identified karst structures—a finding later confirmed by subsequent excavation. Field applications at Wangzhuang and Madaotou coal mines demonstrated its effectiveness in identifying fracture zones, water-rich strata, and fault systems. Repeated measurements across multiple boreholes demonstrated high detection stability and strong consistency with actual exposed geological conditions. Although operational challenges such as signal transmission in narrow spaces and high sampling rate requirements persist, the proposed system successfully balances imaging resolution, operational portability, and real-time processing capability. The results affirm the significant potential of impulse borehole radar for enhancing geological forecasting and improving safety in underground coal mining operations.

Keywords: Borehole Rada; Core Mine; Single Borehole; Impulse Radar

*CORRESPONDING AUTHOR:

Fengjuan Tao, Wuhan Changsheng Coalmine Safety Technology Co., Ltd., Wuhan 430300, China; Email: FJ_Tao@whu.edu.cn

ARTICLE INFO

Received: 8 September 2025 | Revised: 30 October 2025 | Accepted: 4 November 2025 | Published Online: 12 November 2025 DOI: https://doi.org/10.30564/jees.v7i11.11407

CITATION

Wang, Z., Yang, Y., Tao, F., 2025. Single Borehole Detection of Geological Anomalies in Coal Mine Using Impulse Radar. Journal of Environmental & Earth Sciences. 7(11): 20–36. DOI: https://doi.org/10.30564/jees.v7i11.11407

COPYRIGHT

 $\label{localization} \begin{tabular}{ll} Copyright @ 2025 by the author(s). Published by Bilingual Publishing Group. This is an open access article under the Creative Commons Attribution-NonCommercial 4.0 International (CC BY-NC 4.0) License (https://creativecommons.org/licenses/by-nc/4.0/). \\ \end{tabular}$

¹ CHN Energy Shendong Coal Group Co., Ltd., Ordos 01700, China

² Shendong Coal Branch, China Shenhua Energy Co., Ltd., Ordos 01700, China

³ Wuhan Changsheng Coalmine Safety Technology Co., Ltd., Wuhan 430300, China

1. Introduction

Machine Coal resources, as an economical and reliable primary energy source, constitute a major component of China's energy supply^[1]. However, complex geological anomalies such as coal collapse pillars, fractured zones, and faults pose significant challenges for detection and frequently result in mining accidents, compromising safety in underground operations [2-4]. With the advancement of geophysical exploration technologies in underground mining, several coal mines have adopted various geophysical methods for subsurface detection. Currently employed techniques primarily include seismic methods [5,6] and electromagnetic wave methods [7-10], such as, micro seismic monitoring method, transient electromagnetic detection methods, Rayleigh wave exploration, cross-hole electromagnetic wave tomography, and ground-penetrating radar. These methods have shown significant potential in improving detection capabilities. However, each method also presents certain limitations^[11]. For instance, the seismic wave transmission method offers a longer detection range but involves more complex implementation procedures. In contrast, electromagnetic methods are relatively easy to deploy; however, they are highly susceptible to underground environmental interferences (particularly from ferromagnetic materials), resulting in compromised detection accuracy. Borehole radar (BHR) collects data within the borehole, experiences minimal interference from roadway environments, and offers high-resolution capabilities [12], which enable high-precision detection of disaster hazards including coal seam trend prediction and advance small-scale structures, thereby establishing significant application potential for enhancing coal mine safety production.

Borehole radar (BHR) originated in the 1970s^[13–16] in regions including Europe, America, and Japan. It emits electromagnetic waves into the surrounding media, utilizing differences in electrical parameters to infer subsurface structures and physical properties based on direct or reflected wave characteristics. In 1972, Holser et al.^[13] and Cook^[14] successfully developed the first practical borehole radar system, which detected coal resources at depths of up to 100 ft underground, validating the feasibility of electromagnetic wave propagation in coal seams. Sato et al.^[15,16] subsequently advanced a polarized borehole radar system that significantly enhanced imaging capabilities and resolution for

subsurface structures, providing critical technical support for geological exploration. Unlike surface Ground Penetrating Radar (GPR), whose penetration depth is typically limited to a few meters to tens of meters due to the influence of the medium's dielectric permittivity, borehole radar can directly access deep underground through boreholes. This direct subsurface access allows for detection depths of hundreds or even thousands of meters. Thus, in recent decades, borehole radar (BHR)^[17–19] has rapidly evolved into a primary geophysical exploration method in mining operations.

BHR systems can be operated in three primary modes: cross-hole tomography, single borehole-to-surface detection, and single borehole reflection surveys. Figure 1 shows the schemes of the three different modes of BHR systems. The cross-hole radar [20] acquires the radar wave by deploying the transmitting and receiving antennas (dominant frequency: 20-250 MHz) in adjacent boreholes. Based on the acquired radar signals, the spatial distributions of subsurface dielectric permittivity and electrical conductivity can be inverted to interpret geological information between two boreholes. Single borehole-to-surface detection, a configuration formally termed Vertical Radar Profiling (VRP)^[21,22], positions the borehole radar's transmitting antenna to traverse vertically within the borehole at constant velocity—either downward or upward—while multiple receiving antennas are strategically deployed at designated ground positions surrounding the borehole to capture electromagnetic wave propagation. This methodology enables the acquisition of amplitude and velocity tomographic images characterizing the intervening medium between surface receivers and the borehole transmitter. Crucially, VRP achieves substantially greater exploration depths than conventional surface ground-penetrating radar (GPR) by leveraging borehole access to bypass near-surface attenuation layers. However, this technique faces significant operational limitations including stringent site requirements and complex implementation logistics, consequently restricting its practical application in field settings. Single borehole radar^[23,24] can locate geological anomalies situated away from the borehole walls. Compared to cross-hole detection, single borehole detection is more time and cost-saving in both data collection and processing, making it a more feasible and popular approach for investigating geological anomalies at individual pile locations within coal mines.

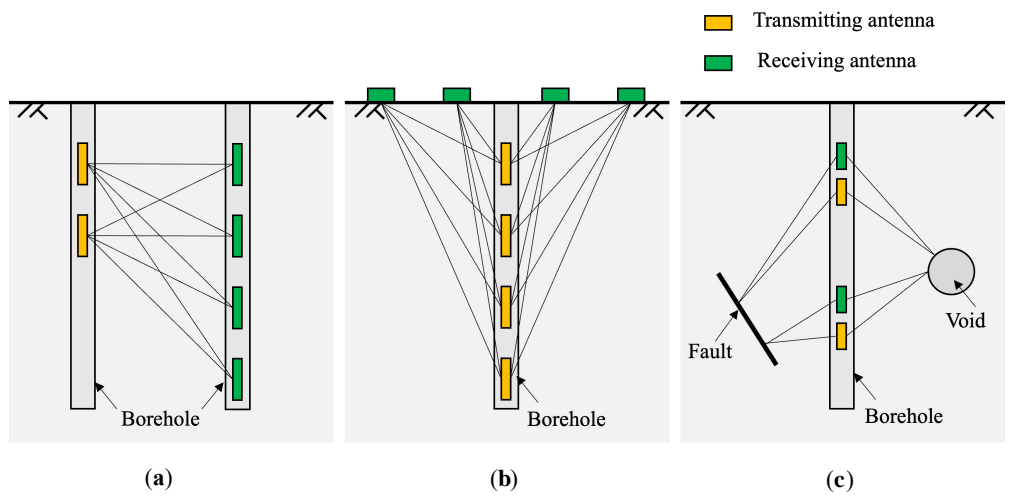


Figure 1. Schemes of the three different modes of BHR systems: (a) cross-hole tomography; (b) single borehole-to-surface detection; and (c) single borehole reflection surveys.

Impulse signals possess wideband characteristics, which endow radar systems based on these signals with high distance resolution, low average power, fast detection speed, and low implementation costs. Such impulse radar systems have found widespread application in the field of remote sensing^[25,26]. However, in the design of impulse borehole radar systems, the pursuit of higher distance resolution necessitates the use of narrower transmitted pulses, which in turn increases the signal bandwidth of the transmitted pulse. This requirement demands a higher sampling rate from the system. Nevertheless, achieving both high sampling rates and precise imaging for borehole radar signals within the confined space of a borehole presents a significant technical challenge. Although equivalent sampling techniques can reduce sampling rate requirements, they substantially compromise logging speed. Furthermore, integrated probe-host configurations utilize specialized logging cables with superior tensile strength but inherent low-pass characteristics. These cables induce severe signal distortion during high-data-rate radar signal transmission, elevate bit error rates, and ultimately constrain both sampled data throughput and command transmission speeds. Due to the physical limitations of boreholes and the complex working environment underground, the operational space for borehole radar in mines is extremely restricted. Additionally, stringent requirements such as explosion-proof design further complicate its deployment. There are inherent trade-offs between radar resolution and sampling rate, as well as between data transmission speed and system compatibility. As a result, the development of borehole radar

systems suitable for detecting complex geological conditions in coal mines still faces numerous challenges.

This paper presents an impulse radar system for single-borehole geological anomaly detection in coal mines. Controlled ground experiments at a railway tunnel validated the system's detection capability and the system's spatial accuracy in geological forecasting. Field applications at two coal mines (Wangzhuang and Maodaotou) demonstrate the system's efficacy in identifying fracture zones, and fault systems. The technology exhibits strong repeatability across multiple detections and shows high consistency with excavated geological conditions.

2. Single Borehole Impulse Radar Detection

2.1. Single Borehole Radar Detection Principle

Borehole radar, as an emerging geophysical detection technology, has demonstrated significant advantages in the field of subsurface exploration. Characterized by its continuity, non-destructiveness, high efficiency, and high precision, it has become an indispensable tool in a variety of application scenarios. The core working principle of borehole radar involves placing a transmitting antenna inside a borehole to emit high-frequency electromagnetic waves into the surrounding medium—typically in the form of wide-band short pulses. In this study, the borehole radar transmits high-frequency electromagnetic waves into the medium in the

form of wide-band short impulses. As these electromagnetic waves propagate through the ground, they encounter interfaces between materials with differing properties, causing a portion of the waves to be reflected. These reflected signals are then captured by a receiving antenna. By precisely processing and interpreting the received signals, borehole radar can effectively detect and locate hidden underground targets.

Figure 2 illustrates the working principle of borehole radar. The transmitting and receiving antennas are placed inside the borehole and automatically scan the surrounding area as they advance at a constant speed. The system emits and receives radar signals in a full 360-degree pattern around the borehole. By analyzing data from a single borehole, it is possible to calculate the distance to and the scale of potentially hazardous geological bodies.

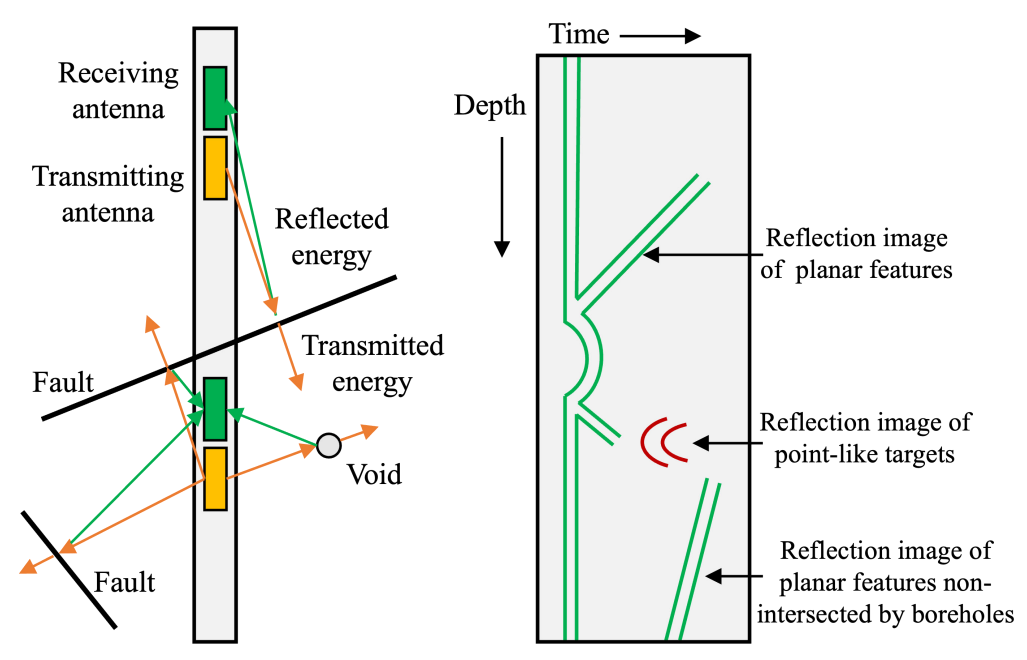


Figure 2. Diagram of single borehole radar detection.

The detection capability of borehole radar relies on the precise mathematical description of electromagnetic wave propagation and reflection characteristics in subsurface media. The distance (H) from an anomaly or interface to the borehole is calculated based on the two-way travel time (TWT) of the electromagnetic wave, which refers to the total time taken for a radar pulse to travel from the transmitter to the target and for its reflected signal to be captured by the receiver. The detailed calculation process is shown in Equation (1):

$$H = \frac{V \times T}{2} \tag{1}$$

Where, H is the distance from the target anomaly to the borehole; V is the propagation velocity of electromagnetic waves in the subsurface medium; T is the two-way travel time (TWT) of the radar signal.

The propagation velocity (V) of electromagnetic waves

in a material medium is always less than its speed in a vacuum and is primarily determined by the electrical and magnetic properties of that medium. The general formula for electromagnetic wave propagation velocity in a medium is shown in Equation (2)

$$V = \frac{C}{\sqrt{\mu_r \varepsilon_r}} \tag{2}$$

Where, V is the propagation velocity of electromagnetic waves in the medium; C is the speed of electromagnetic waves in a vacuum, approximately 3×108 m/s; ε_r is the relative dielectric permittivity (or dielectric constant) of the medium. It is a dimensionless quantity representing a material's ability to store electrical energy relative to a vacuum; μ_r is the relative magnetic permeability of the medium. For most geological materials, μ_r is approximately 1 (i.e., they are non-magnetic), which simplifies the formula as follows:

$$V = \frac{C}{\sqrt{\varepsilon_r}} \tag{3}$$

The detection sensitivity of borehole radar much depends on the difference between the amplitude of the reflected signal and that of the incident signal at the interface between two different media, which can be quantified by the reflection coefficient (R). The reflection coefficient directly related to the contrast in dielectric properties between the two media forming the interface. The reflection coefficient at normal incidence is given by Equation (2) as follows:

$$R = \frac{\sqrt{\varepsilon_{r1}} - \sqrt{\varepsilon_{r2}}}{\sqrt{\varepsilon_{r1}} + \sqrt{\varepsilon_{r2}}}$$
 (4)

Where, R is the reflection coefficient; ε_{r1} is the relative dielectric permittivity of the first medium (e.g., host

rock); ε_{r2} is the relative dielectric permittivity of the second medium (e.g., target geological body). The larger the difference between ε_{r1} and ε_{r2} the greater the reflection amplitude, indicating the more detectable the interface or target.

2.2. The Impulse Radar Prototype System Design

The single borehole impulse radar prototype system, as shown in **Figure 3**, consists of a borehole antenna, a surface computer, a fiber cable, a depth counter, and a charger. The borehole antenna and the surface computer are connected via a wireless Wi-Fi mode, enabling data acquisition, storage, display, processing, analysis, and imaging. The fiber cable passes through the depth counter, which precisely records the depth of the probe.

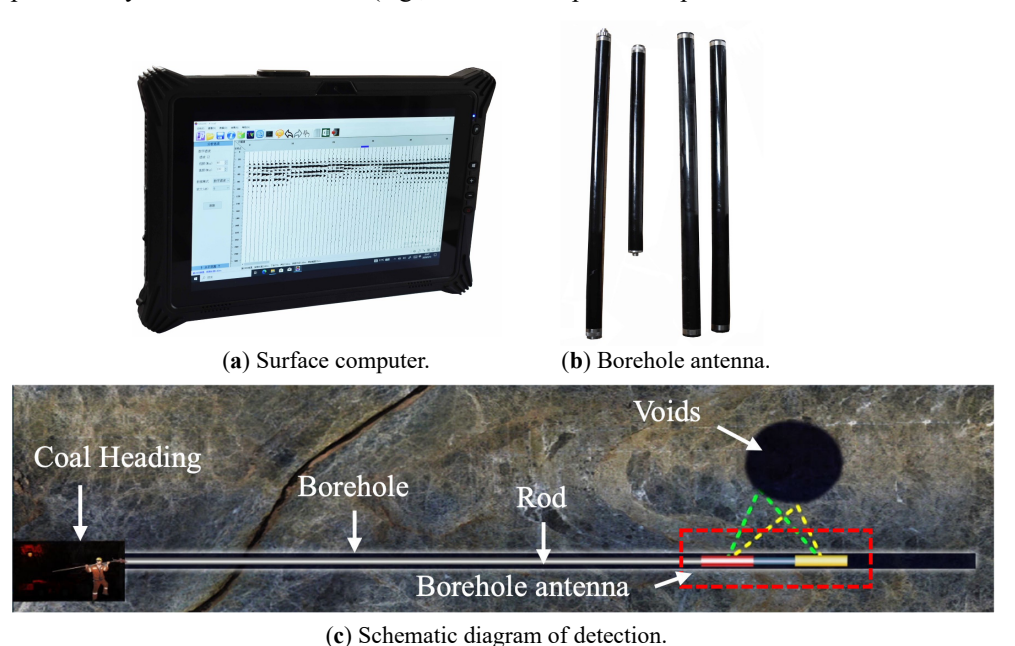


Figure 3. The single borehole BHR prototype system and detection diagram.

To facilitate its use in underground coal mines, the surface computer employs a high-performance, low-power ARM embedded system, powered by a lithium iron phosphate battery pack. To meet the stringent explosion-proof safety requirements of coal mines, the surface computer and the transmitting power supply system are powered by two independent and completely isolated power sources. The human-machine interface is a touchscreen, data export is facilitated via a USB interface, and information is displayed on an LCD screen. The surface computer system primarily comprises optical fiber transceiver and intermediate frequency

modules, as well as a baseband processing module. The intermediate frequency module within the equipment includes a receiving filter, low-noise amplifier, power amplifier, and microwave power detector. Its transmitting end's specific function is to amplify the signal from the baseband module to the power level required by the optical fiber transmitting circuit, thereby meeting the system's detection range requirements. The receiving end's function is to receive signals from the optical fiber receiving circuit, and then perform low-noise amplification and filtering.

The downhole probe is constructed from fiberglass tub-

ing, ensuring its non-conductive and durable properties. The transmitting probe has a diameter of 40 mm, a length of 0.8 m, and a weight of 1.9 kg. The receiving probe has a diameter of 40 mm, a length of 1.4 m, and a weight of 2.8 kg. The equipment is suitable for boreholes with a diameter of 50 mm or more. The probe structure is illustrated in **Figure 4**. The transmitting antenna is an omnidirectional dipole made with two conical copper tubes, and it has a frequency range from 20 MHz to 200 MHz. The receiving antenna shares the same structural design as the transmitting antenna and is equipped with a 24-bit A/D converter.

The transmitting section of the receiving antenna system generates a pulse sequence from the radar host's baseband module encoder. This sequence is then shaped and filtered before being transmitted via optical fiber into the downhole radar probe. After pulse power amplification, the signal is finally emitted by the antenna into the detection area. The receiving section involves the radar probe antenna receiving reflected pulse radio frequency signals from the target area. These signals are then filtered, low-noise amplified, modulated onto optical fiber, and subsequently enter the radar host's baseband digital signal processor for sampling and matched filtering.

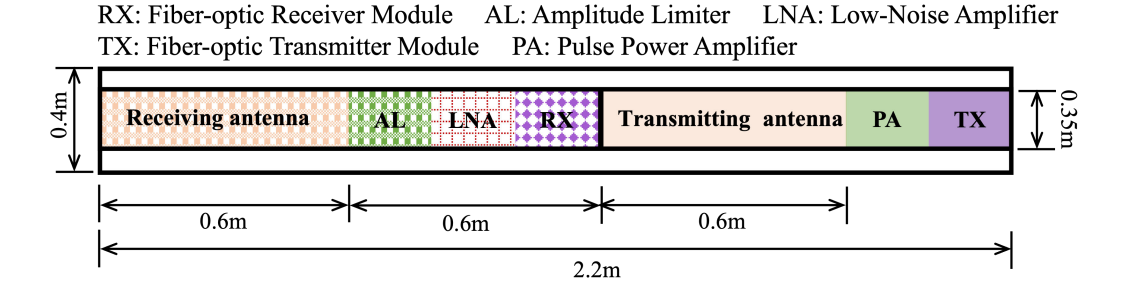


Figure 4. Prototype system and detection diagram.

As depicted in **Figure 3c**, the borehole antenna is pushed uniformly from the borehole mouth to the bottom of the hole using a push rod. During this advancement, the transmitting antenna continuously emits high-frequency broadband electromagnetic waves. These electromagnetic waves propagate circumferentially along the borehole and reflect at impedance interfaces. The reflected waves are then received and pre-processed by the receiving antenna. The resulting electromagnetic wave profile is displayed and analysed by the in-situ computer.

2.3. Validation by a Controlled Ground Experiment

A controlled ground experiment was conducted at a tunnel face on a Railway in west of China. Two boreholes (1# and 2#) were scanned, with depths of 24 m and 30 m respectively, resulting in a total scanned depth of 48 m (effective detection depths: 21 m for cs01, 27 m for cs02). The geometry set is shown in **Figure 5**.

The electromagnetic (EM) wave profiles from the borehole radar experiments for Boreholes 1# and 2# are presented in **Figure 6**. As shown in **Figure 6a**, the borehole radar imag-

ing data for Borehole 1#reveals multiple arc-shaped reflection signals within the scanned section, indicating the presence of karst structures at the following locations: 6.2–9.4 m depth (radius 4.5–5 m), 16–18 m depth (radius 1.5–2.5 m), and 18.3–21 m depth (radius 1–3 m). Notably, the karst feature detected at 18.3–21 m depth shows signs of development along the borehole axis. Additionally, the surrounding rock near the tunnel face appears relatively fractured. Oblique linear reflections observed at 2.2–3.8 m depth (radius 4–6 m) suggest potential fracture zones, while anomalous reflections at 8.4–9.6 m depth (radius 1.5–2.5 m) may indicate fracture development or localized rock fragmentation.

Figure 6a further shows that Borehole 2# radar data exhibits distinct arc-shaped reflections at 19.8–22.6 m depth (radius 1–3 m), confirming a karst structure. The surrounding rock near the tunnel face is also assessed as relatively fractured. Anomalous reflections detected between 8.4–13 m depth (radius 1.5–2.5 m) suggest fracture development or minor fragmentation, while those at 15.6–19 m depth (radius 4.5–5 m) are indicative of a suspected karst structure.

Comprehensive analysis of both boreholes indicates that the karst structure identified in the 6.2–9.4 m range ahead of the tunnel face was only detected in Borehole 1# data. Based on the relative positions of the boreholes, this feature is interpreted to be located on the right side of Borehole 1# (when facing the tunnel face). Field verification is provided in **Figure 7**, showing the photo of the excavated tunnel face 7.2 m

ahead of the working face. The exposed section clearly reveals a karst structure on the right side, validating the accuracy of the integrated borehole radar interpretation and demonstrating its effectiveness in revealing actual ground conditions.

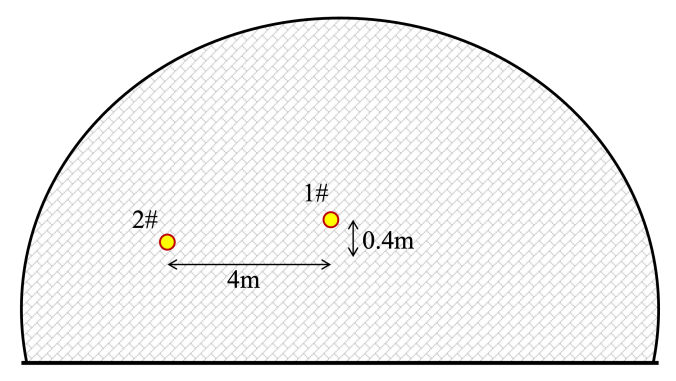
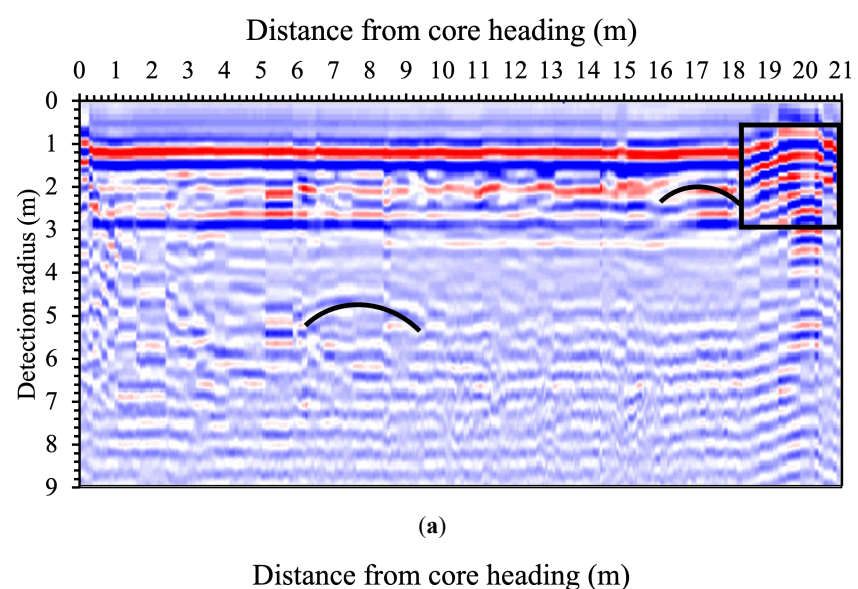


Figure 5. The single borehole detection diagram.



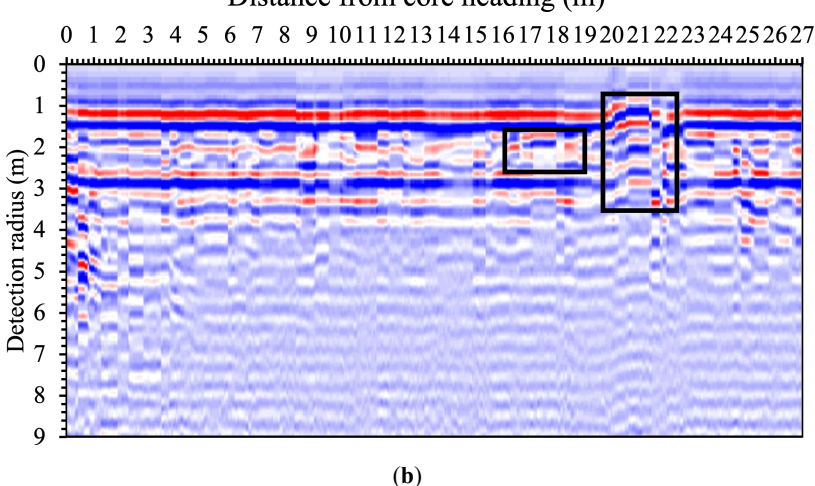


Figure 6. EM wave profiles of BHR experiments in: (a) Borehole 1#; and (b) Borehole 2#.



Figure 7. The photo of the excavated tunnel face 7.2 m ahead of the working face.

3. Field Test

This section presents the field applications of the single borehole impulse radar system in actual coal mine environments.

3.1. Field Case 1: BHR Detection Test at Wangzhuang Mine

3.1.1. General Information

A series of borehole radar detection tests were conducted at the 15112 transportation roadway excavation face in Wangzhuang Coal Mine. This working face is situated in the Permian No. 15 coal seam, with a designed length of 1026 m. The coal seam has an average thickness of 3.75 m, a dip angle ranging from 2° to 4° (averaging 3°), and a burial depth between +895.1 m and +917.9 m. The coal seam at the working face is characterized by a black color and black streak, exhibiting a adamantine luster and conchoidal to step-like fracture patterns, with well-developed endogenic fractures including vertical cracks. It is primarily composed of clarain, followed by durain, interbedded with vitrain bands and minor lenticular fusain, and locally contains fine clay bands along with scattered pyrite nodules and crystals, classifying it as a semi-bright coal. Including one parting measuring 0.20 m in thickness, which is gray-black in color, features argillaceous texture and massive structure, displays even fractures and relatively brittle behavior, and contains occasional plant fossils, the coal seam demonstrates a simple structure and stratigraphically stable position with consistent thickness and minability throughout the entire mine field. The ground surface above the roadway is covered by forests and terraced fields, with minimal impact from engineering activities. The regional geological structure is stable, showing no evidence of magmatic intrusion or fault development. The coal seam structure is simple, containing a single gangue layer with a thickness of 0.20 m.

The coal seam roof consists of mudstone (direct roof, 0.85 m thick) and limestone (old roof, 7.35 m thick). The limestone is identified as the K2 aquifer, characterized by weak water richness, and containing static fissure water. The floor of the coal seam comprises mudstone (direct floor, 1.35 m thick) and fine-grained sandstone (old floor, 1.20 m thick). Detailed information on the coal seam roof and floor is provided in Table 1. The K2 limestone in the old roof serves as a direct water-filling aquifer. Due to geological processes, localized areas of the K2 limestone in the roof exhibit fissure development, containing a certain amount of karst fissure water, primarily in static reserves. The working face floor is located an average of 8.92 m below the K1 aquifer. The hydrogeological assessment indicates a low overall water inflow risk for the working face. The roof strata consist of mudstone (direct roof, 0.85 m thick), the #14 coal seam, limestone (K2 aquifer, old roof, avg. 7.35 m thick), mudstone, and fine-grained sandstone. The K2 limestone serves as the direct water-filling aquifer, characterized by weak water richness and containing static karst-fissure water in locally developed fractures, yet poses no anticipated production impact. Multiple overlying aquifers (K3-K7) are hydraulically isolated by thick mudstone layers. The

floor sequence—mudstone (direct floor, 1.35 m thick) and fine-grained sandstone (old floor, 1.20 m thick)—is situated 8.92 m above the weakly watery K1 aquifer, which also presents no threat. The 15112 haulage roadway advances on a gentle uphill gradient (max 4°) with no water-related con-

cerns. Goaf water in the overlying #3 coal seam is blocked by Permian-Carboniferous impermeable layers, and Ordovician limestone water, with a piezometric level of +656 m to +662 m, lies well below the seam floor elevation of +895.1 m, eliminating any inrush risk.

Layer	Rock	Thickness (m)	Lithology Description
Old Roof	Limestone	6.15 m–8.55 m 7.35 m	Dark gray, thick-bedded, uniform bedding, with irregular fissures observed, no fillings.
Direct Roof	Mudstone	0.35 m-1.35 m 0.85 m	Black, thick-bedded, uniform bedding, incomplete plant fossils.
Direct Floor	Mudstone	0.95 m-1.75 m 1.35 m	Black, thick-bedded, uniform bedding, incomplete plant fossils.
Old Floor	Fine-grained Sandstone	0.85 m-1.55 m 1.20 m	Gray, thin-bedded, wavy bedding, mainly composed of quartz, with minor feldspar and rock fragments, poor sorting, hard.

3.1.2. Detection Test Design

According to the mine's water exploration and drainage design, the test detection boreholes were constructed directly in front of the coal seam, positioned centrally at the roadway face. The designed depth for these boreholes was 60–65

meters, as detailed in **Figure 8**. This industrial test was specifically conducted in borehole 1# of the 15112 working face, involving three in-drilling geophysical surveys, each designed to a depth of 64 m.The detailed drilling parameters for Wangzhuang Coal Mine are presented in **Table 2**.

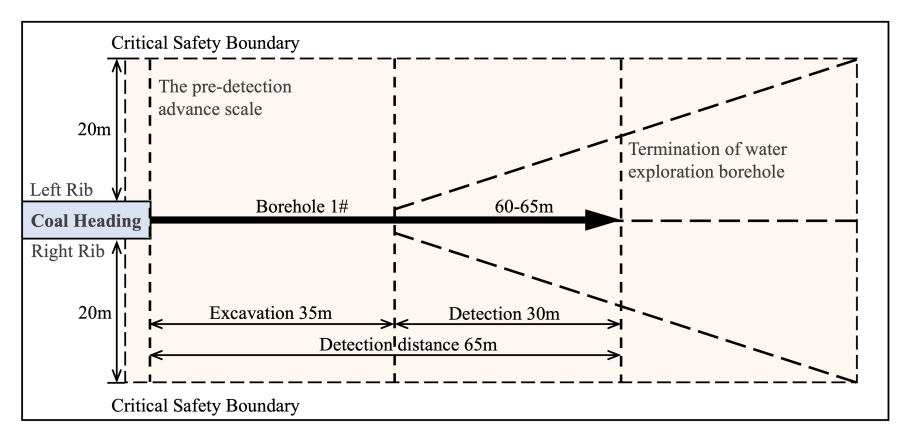


Figure 8. Prospecting Borehole Layout Plan.

Table 2. Wangzhuang Coal Mine Drilling Parameters.

No.	Location	Azimuth	Dip	Depth	
Test 1	788 m north of the entrance of face 15112	0°	6°	64 m	
Test 2	830 m north of the entrance of face 15112	0°	6°	64 m	
Test 3	876 m north of the entrance of face 15112	0°	6°	64 m	

3.1.3. Detection Results and Analysis

Due to borehole collapse, all three borehole radar detection tests were only able to reach depths of 40 to 45 m. The results of these detection tests are presented in **Figures 9**.

Figure 9a shows the results of the borehole radar detection test 1 for Borehole 1# at the 15112 working face,

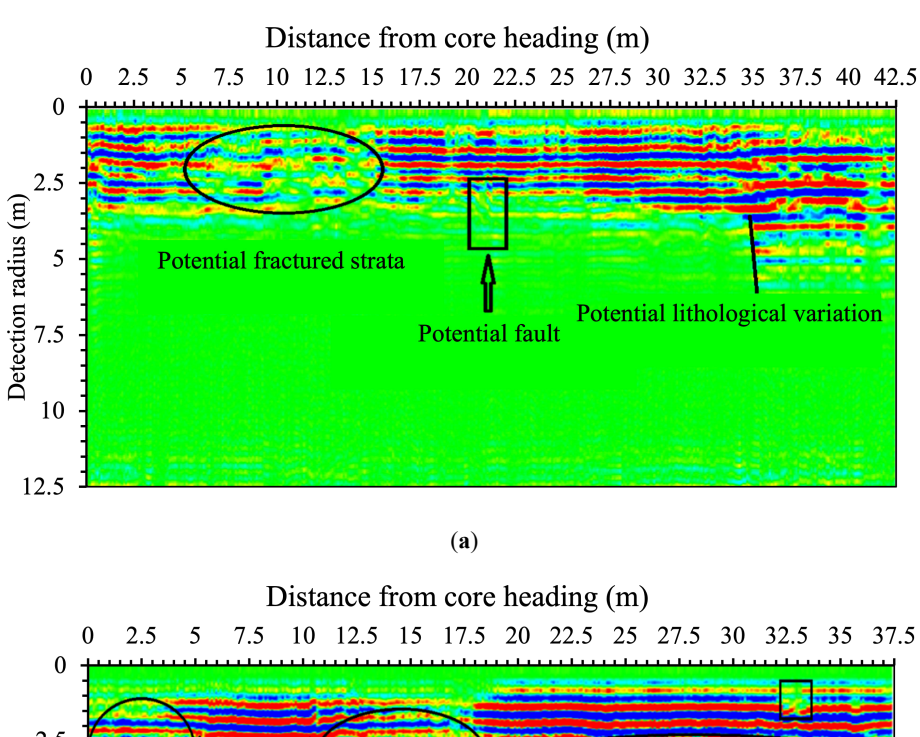
located 788 m north of the opening. As indicated, the entire borehole exhibited no significant geological changes. Signals were relatively weak in the section 5–15 m in front of the borehole, which might suggest relatively fractured rock formations, necessitating attention to potential fissure water seepage. A small structural influence was suspected around 20 m in front of the borehole, beyond a 2.5-meter radius.

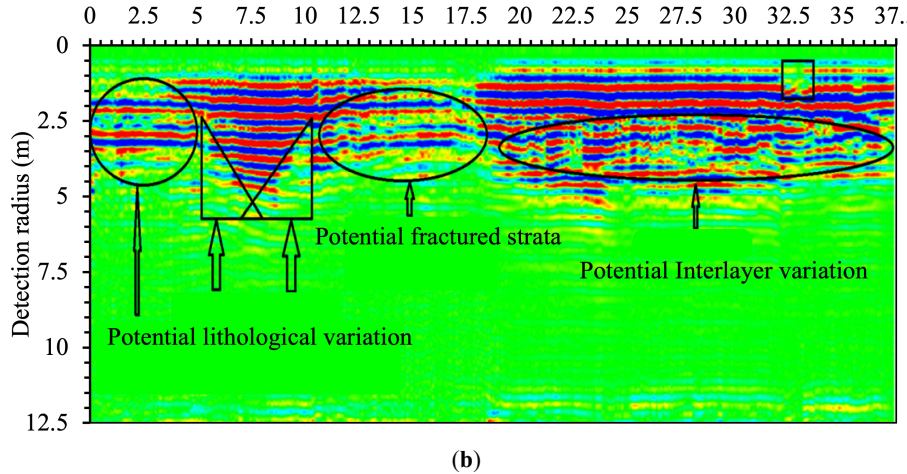
In the 35–41 m section, signals significantly strengthened, possibly indicating changes in rock strata, suggesting that the rock lithology had weak water content. However, radar signals weakened after 42 meters, leading to the inference of potentially strong water content in that section.

Figure 9b shows the results of the borehole radar detection test 2 for Borehole 1# at the 15112 working face, located 816 m north of the opening. As shown, in the range of 0–18 m in front of the borehole, signals alternated, indicating changes in rock strata. Specifically, in the 0–5 m range, the rock formation was fractured, inferring a high water content. This result is consistent with the findings in **Figure 9a** from detection test 1 regarding the possibility of strongly water-bearing rock formation changes after 42 m, demonstrating good repeata-

bility of the radar detection method presented in this paper. Furthermore, in this detection, signals were relatively weak in the 12–18 m range, suggesting rock formation changes or fracturing, and advising appropriate attention to water seepage. A suspected interbed or gangue phenomenon was observed in the 28–37 m range, within a radius of 2.5–5 m.

Figure 9c shows the results of the borehole radar detection test 3 for Borehole 1# at the 15112 working face, located 876 m north of the opening. As indicated, in the range of 27–40 m in front of the borehole, particularly the 38–41 m range, signals were relatively weak. This could be due to relatively fractured rock formations or changes in rock strata, suggesting appropriate attention to fissure water seepage. No significant changes were observed in other detection ranges.





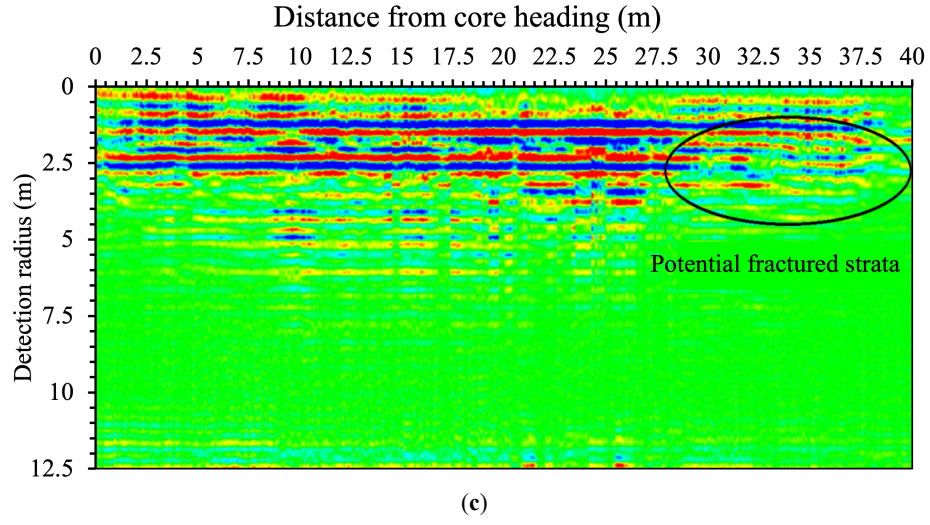


Figure 9. EM wave profiles of BHR test in Borehole 1# at Face 15112: (a) test 1; (b) test 2; and (c) Test 3.

3.2. Field Case 2: BHR Detection Test at cumulative thickness ranging from 0 m to 2.97 m, averaging **Madaotou Coal Mine**1.10 m), primarily composed of gray-black mudstone and

3.2.1. General Information

This borehole radar detection test was conducted in the Face8107-2107 Coal Haulage Gateway. The 8107 working face is situated in the western part of the auxiliary transportation main roadway of the North 1 mining area of Maodaotou Coal Mine. To its west lies the Tiefeng railway protection coal pillar, to its south is the 8106 working face currently under mining, and to its north is the solid coal area, with no goaf above. The designed length of the test roadway is 1440 m, with a burial depth ranging from 1459 m to 1496 m. The surface location of the working face is situated approximately 900 m north of Wangmaozhuang Village and about 280 m east of the Madaotou Railway. The ground surface exhibits well-developed gullies, including one large loess gully. The ground elevation progressively descends from the roadway entrance towards the cutting opening. The area from mileage 0-760 meters is relatively flat woodland, while the section from mileage 760–1440 m features hilly terrain, characterized predominantly by sparse forest and shrubland, with a small portion being farmland.

The 8107 working face exploits the mining targets the 3-5# combined coal seam, which exhibits stable deposition. The coal seam is with a total thickness of 11.98 m to 23.96 m (averaging 19.32 m), and an average pure coal thickness of 18.09 m. The seam contains 0 to 5 layers of gangue (with individual parting thicknesses of 0.14 m to 1.42 m and a

cumulative thickness ranging from 0 m to 2.97 m, averaging 1.10 m), primarily composed of gray-black mudstone and carbonaceous mudstone, with a Protodyakonov coefficient (f) of 3. The coal seam roof consists of weak mudstone/silty fine sandstone (direct roof, 1.16 m thick) and medium-coarse sandstone (old roof, 20.83 m thick). The floor comprises sandy kaolinite (direct floor, 2.67 m thick) and mudstone (old floor, 10.88 m thick). Detailed information on the lithological characteristics and physical-mechanical properties of the coal seam roof and floor is provided in **Table 3**.

Based on the comprehensive hydrogeological assessment, Working Face 8107 is situated under a surface cover of 450-470 m and is traversed by a seasonal loess gully that carries runoff during the rainy season, necessitating ongoing monitoring and surface crack treatment. No overlying Jurassic coal seams or historical small-scale mine workings are present, eliminating the risk of overlying goaf water; however, ongoing observation is required along the 5-m protective coal pillar adjacent to the active Working Face 8106 to the south. The main water-filling source is the Carboniferous Shanxi Formation sandstone fissure aquifer, which lies in close proximity to the coal seam and will drain into the mined-out area following roof collapse. The Ordovician limestone aquifer, located beneath the seam with an average aquifuge thickness of 70 m and a confined water head of 1158 m, exerts a pressure of 1.78-2.28 MPa, resulting in a water inrush coefficient of 0.025-0.033 MPa/m. Overall, this places the working face within a relatively safe zone for confined water mining, with a low overall risk of water inrush.

Table 3	Characteristics of	of Coal Seam	Roof and Floor.

Layer	Rock	Thickness (m)	Lithology Description _	Mechanical Properties (MPa)		
				$\sigma_{ m c}$	σ_{t}	au
Old Roof	Medium-coarse Sandstone	13.35–28.35 20.83	Gray-white, medcoarse grained, massive, gravel-rich base. Quartz/feldspar-dominated with thin siltstone/mudstone.	27.8–46.3	1.42–1.91	0.97–1.37
Direct Roof	Mudstone/Silt- stone	0–2.04 1.16	Gray-white, muddy/fine-grained, massive, quartz/feldspar-dominated.	4.2–13.1	0.11-0.21	0.47-1.03
False Roof	Carb. Mudstone	0–1.12 0.2	Black, muddy, massive, root fossils and coal fragments.	4.1–13.1	0.11-0.21	0.47–1.03
Direct Floor	Sandy Kaolinite	0.7–5.91 2.67	Black, muddy, massive, sandy, plant fossils. Fissures developed.	13.5–27.3	0.88-3.00	1.83–3.57
Old Floor	Mudstone	5.85–19.13 10.88	Gray-white, muddy, massive, few fissures.	4.1–13.1	0.11-0.21	0.47-1.03

^{*} σ_c is the compressive strength; σ_t is the tensile strength; τ is the shear strength.

Locally, the coal thickness is reduced due to lamprophyre intrusion. The surface terrain consists of forests and hills, with loess gullies developed, posing a risk of surface water accumulation during the rainy season. The 2107 roadway revealed two normal faults, with displacements ranging from 0 to 22 m. Specifically, normal fault DF1-120 (H = 0-8 m) is located at chainage 1377 m in the 2107 roadway, and normal fault DF1-111 (H = 0-22 m) is at chainage 1011 m. Fault DF39 (H = 0-15 m) is at chainage 431 m in the 5107 roadway. Near these faults, the coal and rock strata are fractured, joints are well-developed, and the coal seam exhibits a cataclastic structure.

3.2.2. Detection Test Design

This industrial experiment involved a single test with three boreholes, each with a diameter greater than 50 mm. **Figure 10** illustrates the borehole layout plan for the 2107 roadway of the 8107 working face and the location of the fault.

Borehole 1#, 2#, and 3# are respectively positioned 16 m, 32 m, and 48 m in front of the fault. All the three boreholes are at a height of 1 m–1.8 m from the roadway floor and perpendicular to the roadway side, with an elevation angle of approximately 3°. Based on the design analysis, borehole 1# and 2# are expected to intersect the fault at approximately 16–17 m and 37–40 m, respectively. Borehole 3# is not expected to intersect the fault.

3.2.3. Detection Results and Analysis

Figures 11 presents the borehole radar detection results for boreholes 1# to 3# in the 2107 roadway of the 8107 work-

ing face. Figure 11a displays the borehole radar detection image for Borehole 1# at Face8107-2107Gateway. The electromagnetic (EM) wave profiles reveal discontinuous and chaotic signals within the 15.5-17.5 m depth interval, indicating structural discontinuities suggestive of a fault. This finding aligns precisely with the previously documented fault distribution from borehole data. As shown in Figure 11b, Borehole 2# radar detection signals exhibit discontinuity and attenuation between 37.0 m and 45 m depth, suggesting the presence of a fault accompanied by fractured strata and elevated water content. These results show strong agreement with earlier fault mapping derived from borehole investigations. Notably, the fault influence zone identified through borehole radar extends slightly beyond the range previously inferred from geological drilling. Figure 11c demonstrates that Borehole 3# radar signals remain uniform and continuous, indicating no significant geological structures in the vicinity. This detection result is consistent with the design for Borehole 3# that no fault intersections in this working face.

3.3. Discussion

Overall, the proposed single borehole impulse radar system proves to be a highly effective and practical tool for advancing mining safety, as evidenced by its successful application in varied geological settings. The field tests of our single borehole impulse radar system, conducted in a controlled railway tunnel and two active coal mines with distinct geological challenges. The system accurately delineated karst structures in a controlled railway tunnel experiment,

identified zones of potential fracturing and water seepage in the hydrogeologically complex Wangzhuang Mine, and precisely mapped fault zones and their fractured influence areas in the structurally challenged Madaotou Mine. This demonstrates its broad applicability for detecting a range of geological hazards.

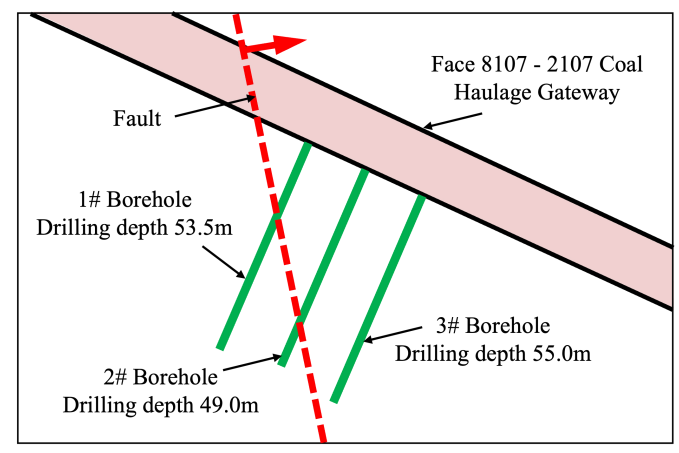
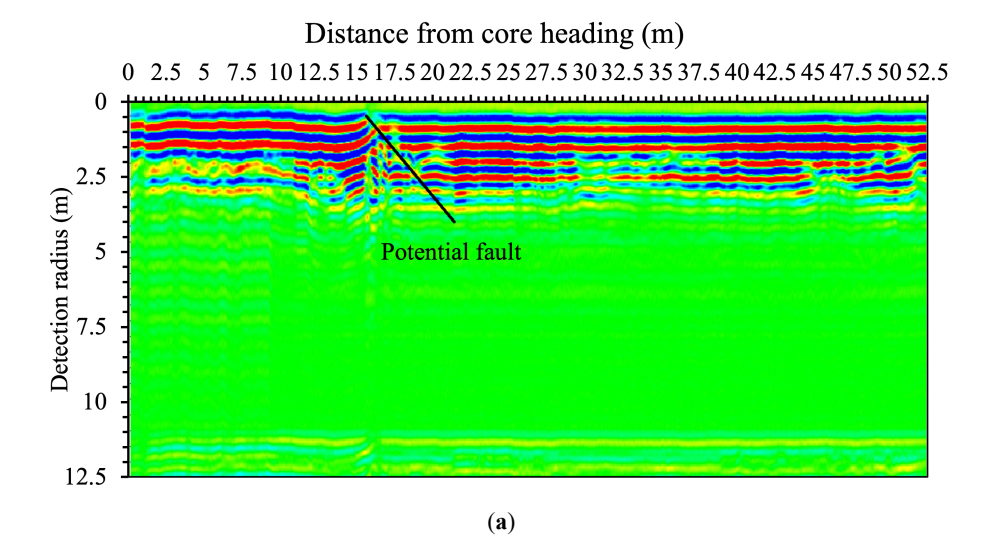
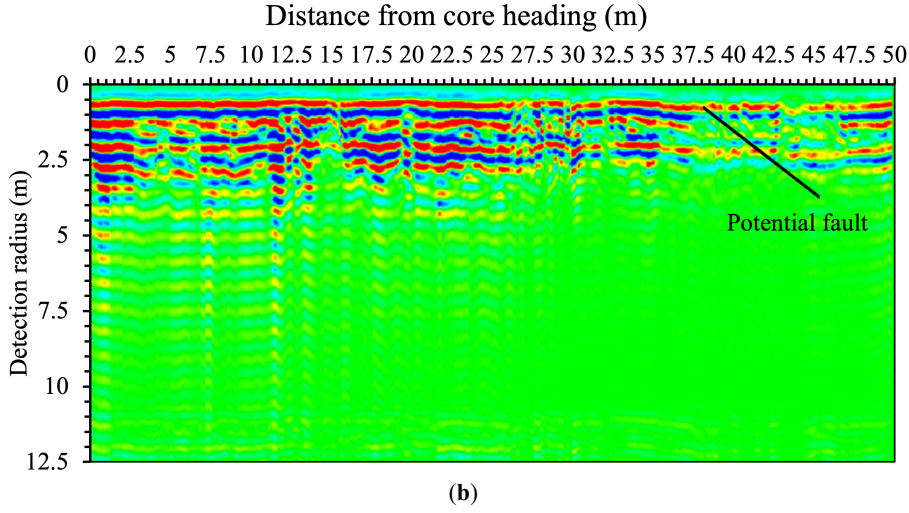


Figure 10. Boreholes layout of Face 8107- 2107 Gateway.





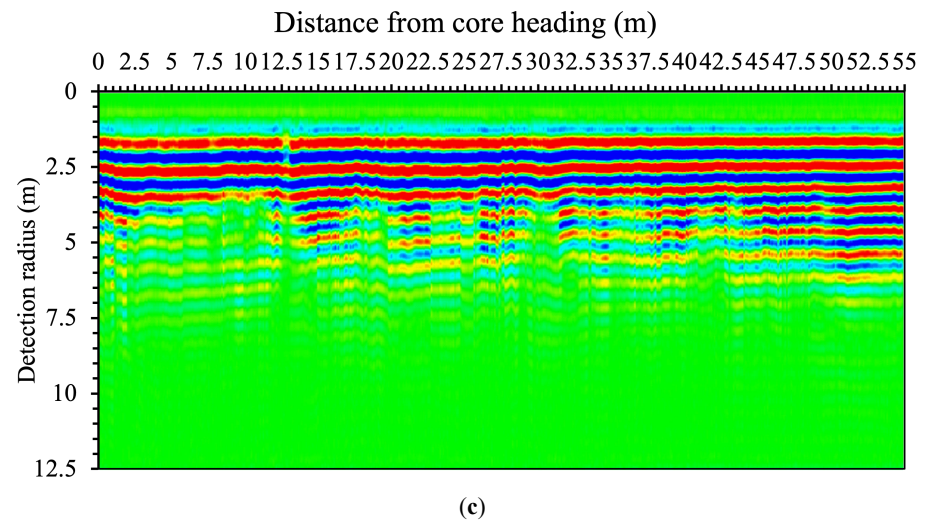


Figure 11. EM wave profiles of BHR test i at Face 8107-2107 Gateway in: (a) borehole 1#; (b) borehole 2#; and (c) borehole 3#.

Compared with existing geophysical techniques, the proposed system demonstrates compelling advantages. Its core advantages of high-resolution, in-situ profiling and operational practicality for underground mines were consistently demonstrated: (1) Its single-borehole reflection mode offers a more logistically straightforward and time-efficient solution for routine advance detection compared to the requirement for multiple, optimally spaced boreholes in crosshole tomography. (2) By operating within the borehole, the system is physically decoupled from the electrically noisy roadway environment, yielding data with a superior signal-tonoise ratio compared to conventional electromagnetic methods deployed in roadways. (3) It successfully bridges the critical gap between the high resolution of surface Ground-Penetrating Radar (GPR) and its limited depth penetration, enabling high-resolution profiling at depths of several tens of meters. Despite the excellent detection performance demonstrated by the borehole radar fine detection and imaging technology in trials at multiple coal mines, the radar signals are susceptible to attenuation or unclear reflections when penetrating the complex geological structures of coal mines due to the influence of heterogeneous media such as groundwater bodies, faults, and goafs. This may consequently compromise the accuracy of the detection results. Besides, the advancement methods of the equipment still face certain limitations in complex environments such as coal mines prone to borehole collapse and confined working spaces. Particu-

larly in mines with high collapse risks, effective detection operations cannot be carried out.

To overcome the limitations of the proposed single borehole impulse radar system and further consolidate the role of pulse borehole radar in proactive mine safety, our future research will focus on improvements in two key aspects: (1) To address the ambiguity in anomaly interpretation, future work will prioritize multi-parameter data fusion. Integrating radar with complementary sensors (such as borehole resistivity or natural gamma probes) will provide independent physical parameters to better discriminate between water, gas, and lithological variations. Simultaneously, developing advanced inversion algorithms capable of jointly interpreting the amplitude, phase, and frequency components of radar signals will enable more quantitative estimation of target properties. (2) Hardware development will aim to enhance borehole compatibility and robustness through probe miniaturization and improved deployment mechanisms, thereby mitigating the impact of unfavorable borehole conditions. In summary, the next-phase research plan focuses on enhancing the adaptability of borehole radar technology in complex environments and advancing its intelligent data analysis capabilities. Through continuous optimization and innovation of these technologies, the project's practical application value and promotion prospects will be further strengthened, ultimately providing more accurate, safe, and cost-effective solutions for fine-scale detection of geological structures in coal mines.

4. Limitations

The main objective of this study was to investigate the single borehole detection of geological anomalies in coal mine using impulse radar. Although, the proposed single borehole detection method was validated using actual excavated sections, multiple field tests, and geological anomalies identified through drilling. We fully acknowledge that relying solely on a single geophysical method represents a limitation of this work. Comparative analysis with additional methods would more convincingly demonstrate the advantages of our approach. Besides, this study primarily employed field case studies to evaluate the effectiveness of the single borehole detection method. The inherent challenges of the field environment restricted the collection of sufficient validation data. A further study is necessary if the proposed method can be successfully applied to real practices with consideration of other geophysical approaches and research methods (i.e., modeling techniques).

5. Conclusions

Based on the development and application of the single borehole impulse radar prototype system, the following conclusions are drawn:

- A robust, portable borehole radar system meeting underground coal mine safety standards was successfully developed. The system features a non-conductive fiberglass downhole probe (transmitting probe: Ø40 mm × 0.8 m, 1.9 kg; receiving probe: Ø40 mm × 1.4 m, 2.8 kg), a surface ARM-based embedded computer with isolated lithium iron phosphate power supplies, and wireless Wi-Fi data transmission. Utilizing omnidirectional dipole antennas (20–200 MHz) with 24-bit A/D conversion, the system is compatible with boreholes ≥ 50 mm diameter and fulfills explosion-proof requirements through fully isolated power systems.
- Controlled ground experiments at a railway tunnel validated the system's detection capability. And, the excavation confirmed a right-side karst structure matching the radar interpretation, verifying the system's spatial accuracy in geological forecasting.
- 3. Field application at Wangzhuang Coal Mine, three radar detection tests were conducted in the 15112 work-

- ing face. Repeated measurements in test 1 and 2 demonstrated good consistency and confirmed the presence of weak and strong water-rich sections at various depths.
- Field application at Maodaotou Coal Mine, single borehole radar detection tests were conducted in three boreholes to verify fault-related geological structures. Boreholes 1# and 2# radar successfully delineated fault locations and influence ranges at 15.5–17.5 m and 37–45 m depths respectively, while Borehole 3# confirmed the absence of faults within its detection range. These results show high consistency with the spatial distribution of faults documented in the three boreholes of the mining face, affirming the system's detection accuracy.

Author Contributions

Conceptualization, Z.W.; methodology, Z.W.; field case, Z.W. and Y.Y.; investigation, Y.Y. and F.T.; data curation, Z.W. and Y.Y.; visualization, F.T.; writing—original draft, F.T.; writing—review and editing, Z.W. and Y.Y. All authors have read and agreed to the published version of the manuscript.

Funding

This work supported by CHN Shenhua Energy Co.Ltd. Shendong Coal Branch (Grant Nos. E210100720).

Institutional Review Board Statement

Not applicable.

Informed Consent Statement

Not applicable.

Data Availability Statement

Some or all data, formulations, or codes generated or used during the study are available from the corresponding author by request. The data contain sensitive information about the mining operations and related parties that could potentially compromise the security and competitive position of the mining company involved. Access to such data is subject to strict regulations and agreements that prevent us

from sharing the raw data outside of the research context.

Acknowledgments

The authors extend their sincere appreciation to Shen Dong Coal Geological Survey Co., Ltd. (a subsidiary of UCHN Energy Investment Group) for their essential support throughout this research initiative. The provision of specialized field access, technical resources, and domain expertise proved indispensable to the successful execution of this study.

Conflicts of Interest

The authors declare no conflict of interest.

References

- [1] Yang, M., 2025. Study on the characteristics of high-frequency electromagnetic wave detection in goaf areas along coal seam borehole. Journal of Environmental & Earth Sciences. 7(7), 259–271.
- [2] Tan, Y., Ma, Q., Liu, X., et al., 2023. Study on the disaster caused by the linkage failure of the residual coal pillar and rock stratum during multiple coal seam mining: Mechanism of progressive and dynamic failure. International Journal of Coal Science & Technology. 10(1), 45.
- [3] Liu, X., Fan, D., Tan, Y., et al., 2021. New detecting method on the connecting fractured zone above the coal face and a case study. Rock Mechanics and Rock Engineering. 54(8), 4379–4391.
- [4] Ullah, M.F., Alamri, A.M., Mehmood, K., et al., 2018. Coal mining trends, approaches, and safety hazards: A brief review. Arabian Journal of Geosciences. 11(21), 651.
- [5] Ge, M., 2005. Efficient mine microseismic monitoring. International Journal of Coal Geology. 64(1–2), 44–56
- [6] Liu, F., Wang, Y., Kou, M., et al., 2024. Applications of microseismic monitoring technique in coal mines: A state-of-the-art review. Applied Sciences. 14(4), 1509.
- [7] Christiansen, A.V., Auken, E., Sørensen, K., 2006. The transient electromagnetic method. In: Kirsch, R. (Ed.). Groundwater Geophysics: A Tool for Hydrogeology. Springer: Berlin, Germany. pp. 179–225.
- [8] Chang, J., Su, B., Malekian, R., et al., 2019. Detection of water-filled mining goaf using mining transient electromagnetic method. IEEE Transactions on Industrial Informatics. 16(5), 2977–2984. DOI: https:

- //doi.org/10.1109/TII.2019.2901856
- [9] Francke, J., 2012. A review of selected ground penetrating radar applications to mineral resource evaluations. Journal of Applied Geophysics. 81, 29–37. DOI: https://doi.org/10.1016/j.jappgeo.2011.09.020
- [10] Slob, E., Sato, M., Olhoeft, G., 2010. Ground-penetrating radar: Surface and borehole ground-penetrating-radar developments. Geophysics. 75(5), 103–120.
- [11] Xu, X.L., Zhu, X.S., Li, T.T., et al., 2025. Research on directional detection technology of mine borehole radar. Journal of Mining Science and Technology. 10(1), 14–23. (in Chinese)
- [12] Liu, L., Shi, Z., Peng, M., et al., 2020. Investigation of geological anomalies at pile foundation location in urban karst areas using single borehole radar. Geosciences. 10(6), 232. DOI: https://doi.org/10.3390/ge osciences10060232
- [13] Holser, W.T., Brown, R.J.S., Roberts, F.A., et al., 1972. Radar logging of a salt dome. Geophysics. 37(5), 889–906. DOI: https://doi.org/10.1190/1.1440307
- [14] Cook, J.C., 1977. Borehole-radar exploration in a coal seam. Geophysics. 42(6), 1254–1257. DOI: https://doi.org/10.1190/1.1440790
- [15] Sato, M., Tanimoto, T., 1992. A shielded loop array antenna for a directional borehole radar. In Proceedings of the Fourth International Conference on Ground Penetrating Radar, Rovaniemi, Finland, 1992.
- [16] Sato, M., Ohkubo, T., Niitsuma, H., 1995. Cross-polarization borehole radar measurements with a slot antenna. Journal of Applied Geophysics. 33(1–3), 53–61.
- [17] Zhong, S., Wang, C., Wu, L., et al., 2012. Borehole radar response characteristics of point unfavorable geo-bodies: Forward simulation of its surrounding rock and filling condition. Rock and Soil Mechanics. 33, 1191–1195.
- [18] Ma, C., Zhao, Q., Wang, L., et al., 2015. Modeling borehole radar by finite-difference time-domain in conductive sandstone. Journal of Environmental and Engineering Geophysics. 20(1), 19–29. DOI: https://doi.org/10.2113/JEEG20.1.19
- [19] Ebihara, S., 2004. Directional borehole radar with dipole antenna array using optical modulators. IEEE Transactions on Geoscience and Remote Sensing. 42(1), 45–58. DOI: https://doi.org/10.1109/TG RS.2003.818113
- [20] Liu, S., Liu, X., Meng, X., et al., 2018. Application of time-domain full waveform inversion to cross-hole radar data measured at Xiuyan jade mine, China. Sensors. 18(9), 3114. DOI: https://doi.org/10.3390/ s18093114
- [21] Cassiani, G., Strobbia, C., Gallotti, L., 2004. Vertical radar profiles for the characterization of deep vadose zones. Vadose Zone Journal. 3(4), 1093–1105.

- [22] Tronicke, J., Hamann, G., 2014. Vertical radar profiling: Combined analysis of traveltimes, amplitudes, and reflections. Geophysics. 79(4), H23–H35.
- [23] Zhao, J.G., Sato, M., 2006. Radar polarimetry analysis applied to single-hole fully polarimetric borehole radar. IEEE Transactions on Geoscience and Remote Sensing. 44(12), 3547–3554.
- [24] Bici, J., 2024. Using borehole radar detecting hydraulic fracturing crack in near horizontal holes in
- coal mine. Frontiers in Earth Science. 12, 1253315. DOI: https://doi.org/10.3389/feart.2024.1253315
- [25] Yang, H., Li, T., He, Z., et al., 2014. Impulse borehole radar imaging based on compressive sensing. IEEE Geoscience and Remote Sensing Letters. 12(4), 766–770.
- [26] Dang, L., Yang, H., Teng, B., 2018. Detection imaging of impulse borehole well-logging radar. EURASIP Journal on Image and Video Processing. 2018(1), 105.